

## TWO-DIMENSIONAL VELOCITY STRUCTURE ALONG THE SYNCLINAL AXIS OF THE GREAT VALLEY, CALIFORNIA

BY ROBERT H. COLBURN AND WALTER D. MOONEY

### ABSTRACT

In 1981 and 1982, the U.S. Geological Survey conducted a seismic refraction study of the Great Valley, central California, in order to obtain a better understanding of the deep crustal structure and tectonic evolution of the region. We present the interpretation of a 147-km-long seismic refraction profile recorded along the synclinal axis of the Valley. The northern 98 km of the profile are reversed, whereas the remaining southern portion is unreversed. Observed travel times and amplitudes of primary and secondary arrivals from three shot points have been modeled using two-dimensional ray tracing techniques. The resultant *P*-wave velocity cross-section consists of a 27-km-thick crust whose isovelocity contours generally rise gently to the southeast. The crust is described in six layers, with average velocities (average layer thickness in parentheses) of 2.8 km/sec (3 km), 4.25 km/sec (3 km), 5.5 km/sec (2 km), 6.1 km/sec (6 km), 6.75 km/sec (6 km), and 7.2 km/sec (7 km). The second through fifth layers are separated by 1-km-thick high gradient transition zone; the lower crustal boundary (6.75/7.2 km/sec) and the Moho (7.2/8.1 km/sec) are modeled with first-order discontinuities. The first layer (Cenozoic sedimentary deposits) is characterized by a velocity gradient of 0.7 km/sec/km starting with a velocity of 1.7 km/sec at the surface. The second layer (4.25 km/sec) consists of the Cretaceous Great Valley Sequence and shows a very modest velocity gradient of 0.2 km/sec/km. The third layer (5.5 km/sec; "basement") may consist of metasedimentary rocks of the Franciscan assemblage, fractured crystalline rocks, or possibly serpentized ophiolite. The fourth layer (6.1 km/sec) apparently has no velocity equivalent 30 km to the west in the Diablo Range; it and the layer beneath it (6.75 km/sec) may be correlated with the metamorphic and igneous rocks of the eastern foothills of the Sierra Nevada. The basal crustal layer (7.2 km/sec) is evidently mafic igneous rock. An independent interpretation of this profile using the reflectivity method produced a similar model. An interpretation of a parallel profile 10 to 15 km east of our line shows a structure similar to our model below 15 km, but a thinner sedimentary section and velocities as much as 0.9 km/sec faster 6 to 15 km deep. The crustal velocity structure of the central Great Valley is atypical of either continental or oceanic crust, but is consistent with the geologic hypotheses that the Valley is a thickened marginal basin, formed in either a forearc or backarc setting located west of the Mesozoic Sierra Nevada arc.

### INTRODUCTION

In 1981, the U.S. Geological Survey (USGS) initiated a geologic and geophysical investigation of the crustal structure and evolution of central California. Interest in this investigation arose for several reasons. First, in the context of plate tectonics, this region is interpreted to represent an archetypal trench-forearc basin-volcanic arc ensemble (i.e., Franciscan assemblage-Great Valley-Sierra Nevada; Dickinson, 1976). The determination of the deep crustal structure of this common tectonic ensemble is important to understanding its evolution in California and where it occurs elsewhere, world-wide. Second, because the region includes the Pacific-North American plate boundary, it is a region of active tectonic processes and of correspondingly high seismic risk. This risk is not limited to earthquakes occurring on the San Andreas fault; the  $M = 6.2$  earthquake near the city of Coalinga, California,

on 2 May 1983 highlights the potential for seismic activity at the Great Valley-Coast Range boundary as well.

Seismic refraction measurements of crustal velocity structure are an important aspect of the ongoing USGS central California investigation. The profile reported here is one of two axial profiles which, for the first time, provide details on the crustal structure in the central Great Valley.

#### PREVIOUS WORK

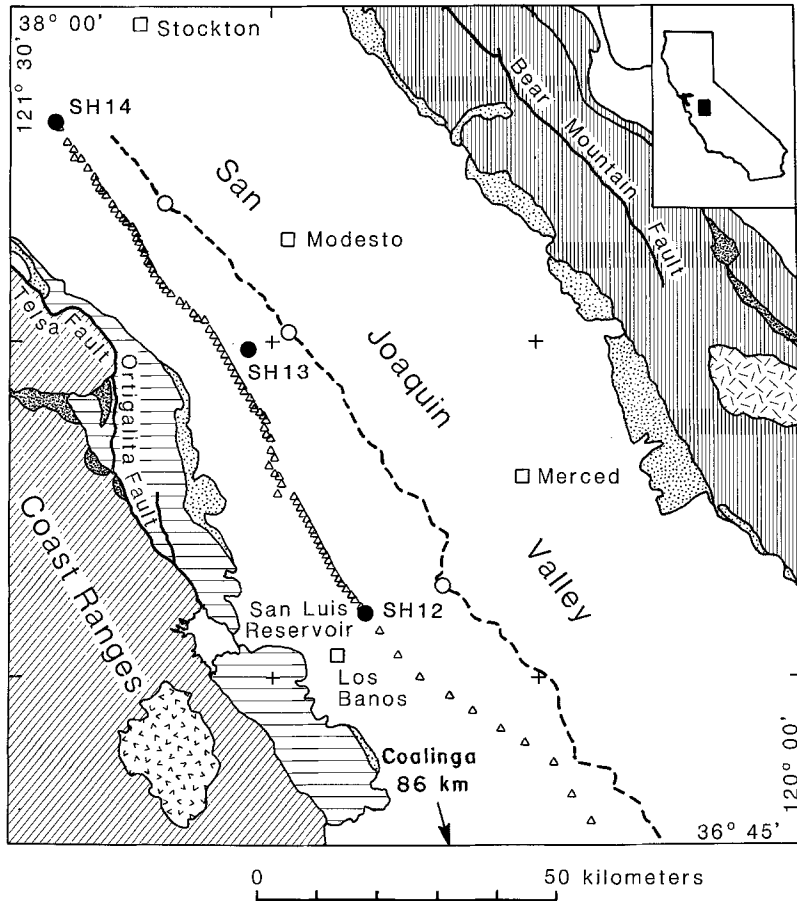
Seismic refraction measurements of the crustal velocity structure of central California have been made since the early 1960's. Profiles parallel to the geologic strike were recorded in the Coast Ranges on either side of the San Andreas fault (Healy, 1963; Stewart, 1968) and in the Sierra Nevada (Eaton, 1966; Prodehl, 1979). In addition, two profiles were recorded across the geologic strike at the latitudes of San Francisco and San Luis Obispo (Eaton, 1963, 1966). Together, these profiles sufficed to determine the gross features of the crustal structure. They show a 24- to 29-km-thick crust in the central Coast Ranges which thickens to the east, reaching 40 to 55 km beneath the Sierra Nevada. Since no profiles were recorded parallel to the axis of the central Great Valley, the crustal structure there has been inferred from the sparse data on the cross-profiles and especially from the potential field data. Cady (1975) estimated a crustal thickness of 30 km from gravity and aeromagnetic data and concluded that much of the crust of the Great Valley is underlain by dense, mafic crust of probable oceanic origin. The present study tests this hypothesis.

The seismic refraction profile presented here is part of a large set of refraction and reflection profiles recently recorded in central California (Wentworth *et al.*, 1984, 1985). Holbrook and Mooney (1986) present the interpretation of a seismic refraction profile parallel and 10 to 15 km east of the present profile; we compare our results with theirs below. Three seismic refraction profiles (Whitman *et al.*, 1985) and a reflection profile (Zoback and Wentworth, 1985) cross the Great Valley perpendicular to the present profile, and are currently being interpreted. The present profile, which is parallel to the geologic strike, provides important constraints on the interpretation of these cross-to-strike profiles.

#### DATA

One hundred portable seismographs were deployed to record the profile. Each seismograph consists of a 2-Hz geophone whose output is recorded in multiplexed FM format on a cassette tape at three gain levels. Timing is provided by internal chronometers which are set to a master clock before deployment and are rated for drift after the seismographs are retrieved.

Three shots were fired into the seismograph array (Figure 1, Table 1). These are numbered shot (SH) 14 at the north, SH 13 in the middle (48 km southeast of SH 14), and SH 12 at the south (96 km southeast of SH 14). The seismographs were deployed at about 1 km spacing between the end shot points; spacing was increased to about 5 km spacing southeast of SH 12. Each shot consisted of an 8-inch drill hole that was 45 m deep and loaded with 800 kg of ammonium nitrate explosives. The shots were electronically detonated by the same master clocks used for seismograph timing. Timing for both seismographs and shots is accurate to 0.005 sec. Seismograph and shot point locations were determined on 1:24,000 topographic maps by visual inspection and are accurate to 15 m. The analog data are digitized at 200 samples/sec at the USGS office in Menlo Park. The record sections analyzed in this study are shown in Figure 2 in trace-normalized format.



## EXPLANATION

Quaternary Sedimentary Rocks	Ultramafic Rocks
Tertiary Sedimentary Rocks	Granitic Rocks
Tertiary Volcanic Rocks	Mesozoic Metamorphic Rocks
Mesozoic Great Valley Sequence	Seismograph location
Franciscan Assemblage	Shot point
	Parallel refraction profile

FIG. 1. Generalized geologic map (after Jennings, 1977) showing the location of the west Great Valley, California, seismic refraction profile. Dots indicate shot locations, and triangles indicate station locations. Dashed line indicates location of profile interpreted by Holbrook and Mooney (1986). Note that SH 13 is offset 3.85 km northeast of the nearest recorder on the western profile. Southeast of SH 12, the station spacing increases to 5 km, and the trend of the line is more easterly.

## INTERPRETATION METHOD

The three record sections recorded along this profile have been interpreted using two-dimensional ray trace modeling techniques. This procedure consists of constructing an initial two-dimensional velocity model by combining one-dimensional velocity models calculated for each shot, and iteratively modifying this initial model until it matches the arrival times and amplitudes for all three shots. We assumed we would determine a fairly uniform velocity structure of moderate dips and lateral

velocity variations since the profile parallels the geologic strike, and because the major seismic phases correspond on the three record sections. The amplitudes of the seismic phases form an important constraint on the forward modeling process for velocity structure. These amplitudes have been modeled by generating synthetic seismograms that were calculated from the geometrical ray theory method formu-

TABLE 1  
SHOT LOCATIONS

Shot No.	Latitude			Longitude		
	(deg)	min	sec)	(deg)	min	sec)
12	37	05	49.4	120	49	46.4
13	37	29	17.2	121	02	46.5
14	37	49	36.1	121	24	37.9
Location 746*	37	28	16.3	121	05	3.3

\* Closest recorder to SH 13 (offline shot).

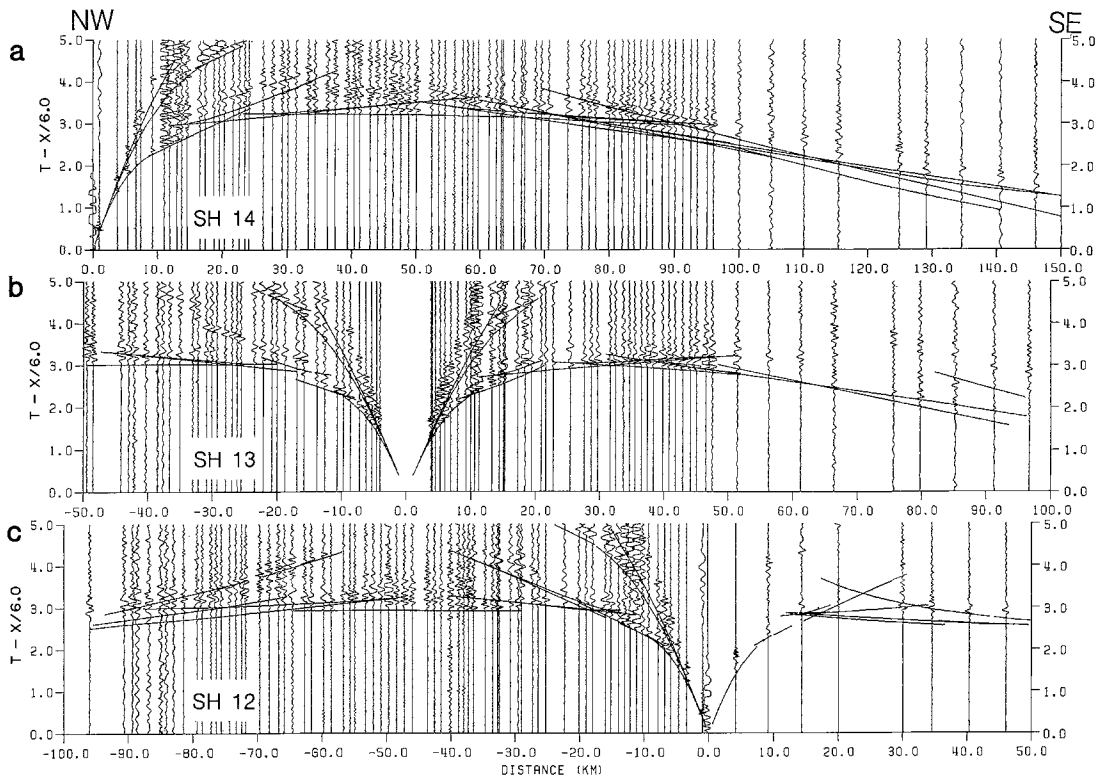


FIG. 2. Normalized record sections with calculated travel times superimposed for: (a) SH 14, (b) SH 13, and (c) SH 12. These and all other record sections are plotted with a reduction velocity of 6.0 km/sec. Travel times are calculated from the velocity models of Figure 3.

lated by McMechan and Mooney (1980). The 1 km station interval would resolve any major features greater than 2 to 3 km in length in the upper 10 km of the crust.

One of the most prominent features of this data set are the high-amplitude, free-surface multiple refractions. These phases are refracted in the sedimentary column and reflected at the free surface one or more times (c.f. Fuis *et al.*, 1984). In the present study, we model these phases with ray theory. Hwang and Mooney (1986) present wave theory modeling of these same phases.

Several factors contribute to uncertainties in the analysis. Uncertainties in locations and in shot and instrument timing result in negligible errors that are less than the 5 msec sampling rate of the digitized traces. Greater errors result when picking arrival times from each trace. For this data set, which has a favorable signal-to-noise ratio, we estimate uncertainties in travel times to be  $\pm 0.01$  sec for near-surface-refracted arrivals,  $\pm 0.05$  sec for mid-crustal refracted arrivals, and  $\pm 0.08$  sec for all reflected phases. Since dense station spacing provides a high sampling rate for various phases, we estimate uncertainties in the apparent velocities to be on the order of  $\pm 0.1$  km/sec. While we have no physical way of knowing how close our model approximates the "real earth," testing depths to interfaces for our models using the above error analysis results in uncertainties on the order of  $\pm 0.05$  for near-surface boundaries,  $\pm 0.3$  km for mid-crustal boundaries, and  $\pm 0.5$  km for deep crustal boundaries. Amplitude modeling provides further constraints on velocity gradients and on velocity contrasts between layers. One must remember that the depth to an interface is constrained only where it is sampled by rays which are reflected or which turn up from their greatest depth.

TABLE 2  
DISTANCES BETWEEN SHOT POINTS IN KILOMETERS

	SH 12	Location 746*	SH 13	SH 14
SH 12		47.267	47.461	95.973
Location 746*	47.267		3.850	48.845
SH 13	47.461	3.850		49.452
SH 14	95.973	48.845	49.452	

\* Closest recorder to SH 13.

SH 13, the center shot point, was offset from the profile 3.85 km east of the nearest recorder (site 746; Figure 1). Table 2 lists distances between shot points, and distances between shot points and site 746. Because there was no recorder at SH 13, there is no reciprocal travel time recorded to SH 13 from either SH 14 or SH 12. The travel time of the first arrival from SH 14 to site 746 is 0.19 sec later than from SH 13 to SH 14, and the travel time from SH 12 to site 746 is 0.11 sec later than from SH 13 to SH 12. Therefore, we present our interpretation as follows. First, we discuss our preferred model between the two reversed shots, SH 12 and SH 14 (model M12-14). Next, we present a slightly modified version of the model that is fitted to the data from SH 13 (model M13). Finally, we discuss the models for the unreversed southern section of our profile, southeast of SH 12. Figure 3 shows the upper 21 km of both models.

#### SH 12 AND SH 14

Our preferred velocity model, model M12-14 (Figure 3a) shows a fairly simple structure which dips slightly to the northwest. Between the shot points, the sedimentary column (velocity less than 5.0 km/sec) extends to about 6.0 km depth, with deeper velocity discontinuities at about 8.5, 16, and 19.5 km. Moho occurs at a depth of 27 km and is not shown on this figure for reasons of scale. Figures 4 and 5 show the record section data, ray trace diagrams, and synthetic record sections for SH 12 and SH 14. The data are plotted in true amplitude format, i.e., each trace is corrected for amplifier gain and is scaled by the square of the distance to correct for geometrical spreading and the effects of scattering and attenuation.

*Upper crust.* The surficial velocities of the sedimentary deposits range from 1.65 to 1.9 km/sec. The prominent free-surface multiples and the arcuate travel-time curve A (Figures 4 and 5) indicate a high gradient to about 3 km depth, where the velocity ranges from 3.85 to 4.1 km/sec. At 3 km depth, there is an 0.5-km-thick lower gradient layer with the velocity ranging from 4.1 to 4.2 km/sec. This is seen

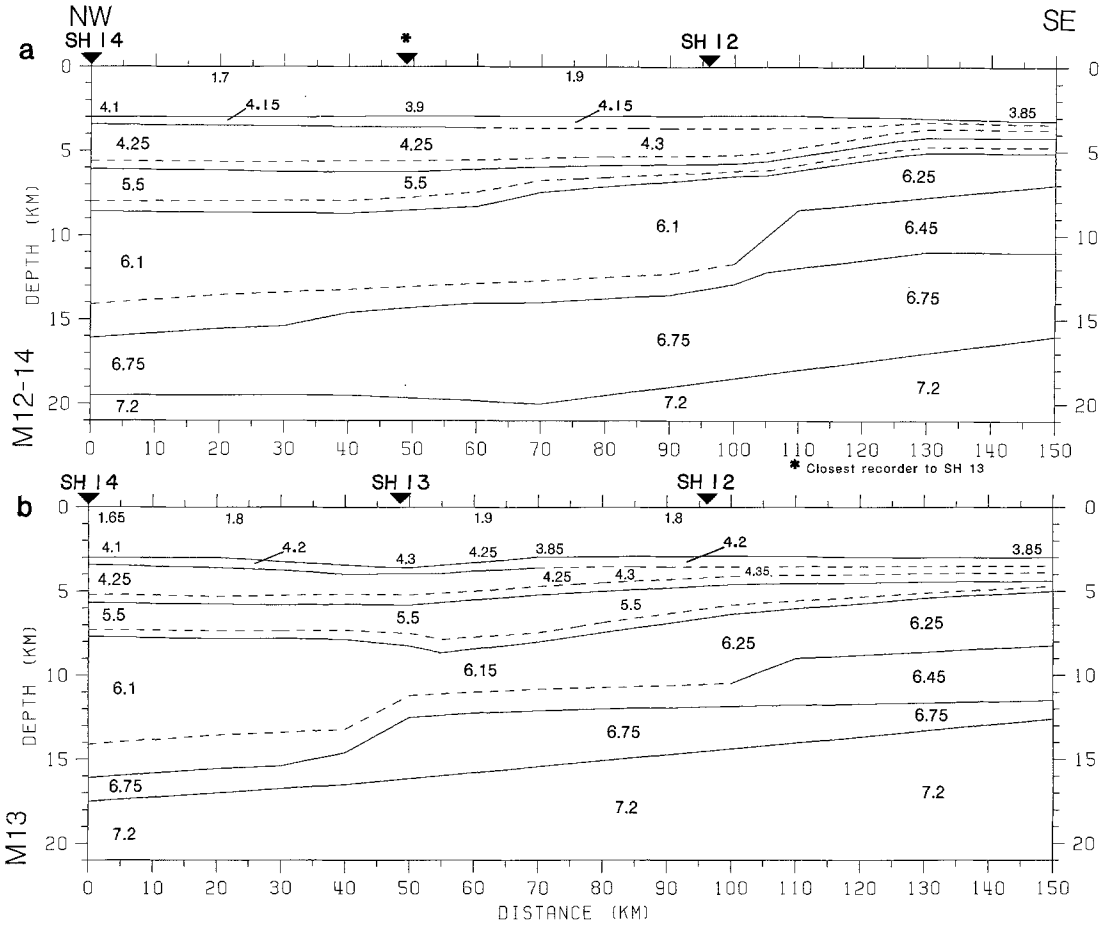


FIG. 3. Two-dimensional velocity models: (a) M12-14 (the preferred model which fits the SH 12 and SH 14 data), and (b) M13 (which fits data from the offline SH 13). The upper 21 km of both models are shown at a vertical exaggeration of 2.5:1. Average layer velocities are indicated in kilometers/second. Solid interfaces indicate velocity discontinuities. Dashed interfaces are isovelocity contours that indicate the tops of high-gradient velocity transition zones at the base of the 4.3 km/sec layer, the 5.5 km/sec layer, and the 6.1 km/sec layer. Velocity-depth functions for these models are shown in Figure 6, and the numerical values are tabulated in Table 3. Depths to major crustal boundaries are generally shallower for model M13 as compared to model M12-14, as is consistent with the well-determined eastward updip of the Valley basement.

as the linear travel time curve B, which extends out to about 15 km from the shots. Beyond this distance, first arrival amplitudes decay abruptly on travel-time curve C (Figures 4 and 5), suggesting the presence of a modest low-velocity zone below the 4.2 km/sec layer. This amplitude decay is more noticeable from SH 14 than from SH 12. Further evidence for this low-velocity zone is a noticeable time delay of the basement reflection (phase D, Figure 4). We have modeled this low-velocity zone with velocities ranging from 4.15 km/sec at 3.5 km depth to 4.35 km/sec at about 5.5 km depth. At the south end of model M12-14, where the amplitude decay

is not so prominent, this layer is modeled as an abrupt change in gradient (without a low-velocity zone), with the velocity ranging from 4.25 to 4.35 km/sec.

The transition from sedimentary to basement rocks is modeled by a high-velocity gradient zone ranging in depth from 5.5 to 6.0 km. Without a transition zone, the

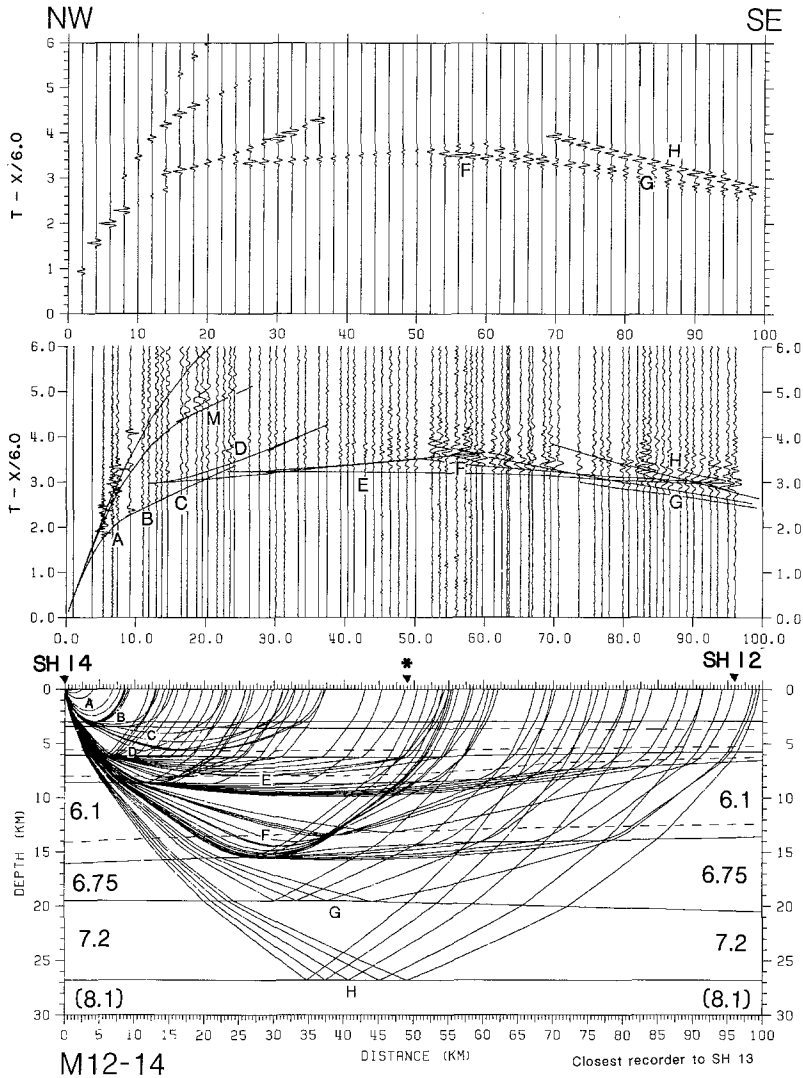


FIG. 4. (SH) 14: Synthetic seismogram record section (*top*), true amplitude record section scaled by distance squared (*middle*), and ray trace diagram (*bottom*) for model M12-14. The travel-time curves are superimposed on the record section calculated from the model shown. Velocities shown are average velocities in kilometers/second within each layer. Phases A and B are first arrivals that travel through the near-surface sediments. Phase C denotes an abrupt decrease in first arrival amplitudes interpreted to be caused by a thin, low-velocity zone within the sediments. Phase D is the reflection off the top of the basement. Phase E denotes the 6.1 km/sec travel-time curve, near where it crosses over from the 5.5 km/sec travel-time curve. Phase F is the refraction through the transition zone between the 6.1 km/sec layer and the 6.75 km/sec layer. Phase G denotes arrival reflected off the interface at 20 km depth, and phase H denotes arrivals reflected off the Moho at 27 km depth. Estimated mantle velocity is 8.1 km/sec. Phase M denotes the near-surface multiple.

velocity contrast between the sediment and basement rocks would be high (from 4.35 to 5.5 km/sec), resulting in a larger amplitude reflection than observed in the data. The use of a transition zone at the base of the sediments decreases the amplitudes of the basement reflector in the synthetic seismograms so that they

more closely match the data. The calculated amplitudes for phase D from SH 14 are larger than seen in the data; this discrepancy is even greater without the transition zone.

Cross-over to a basement velocity of 5.5 km/sec occurs at about 22 km from both SH 14 and SH 12. A change in the apparent velocity from 5.5 to 6.1 km/sec occurs

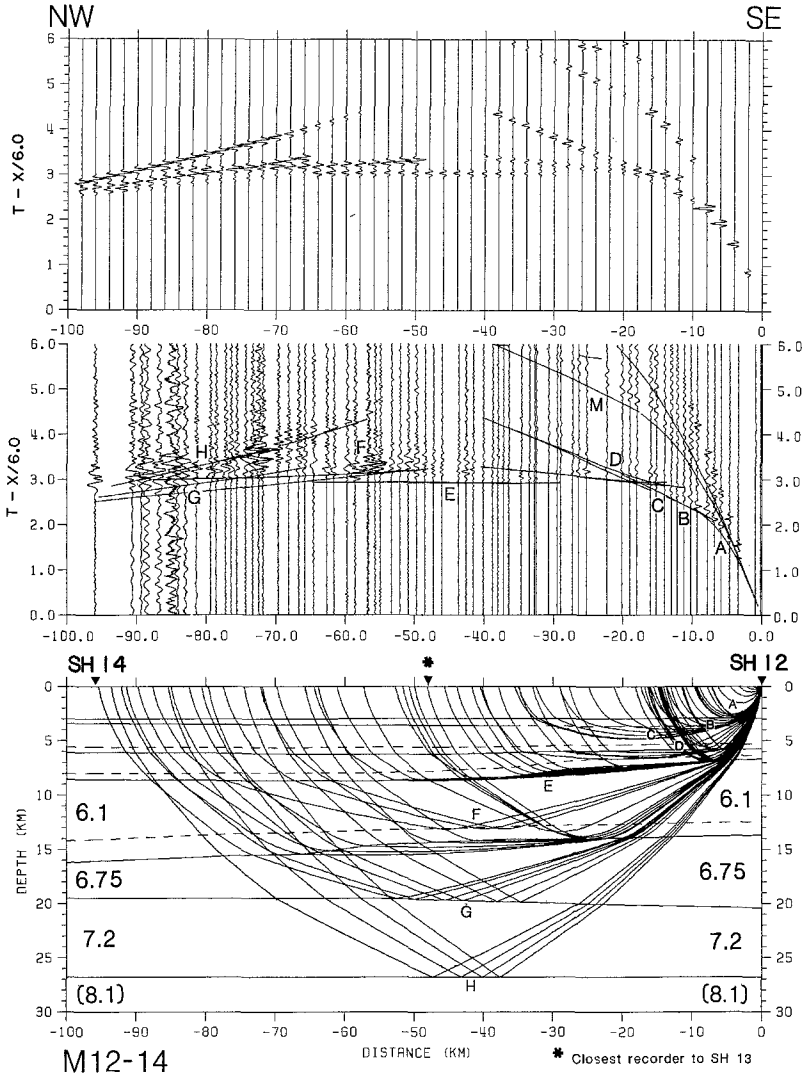


FIG. 5. (SH) 12: Synthetic seismogram record section (top), true amplitude record section and labeled by distance squared (middle), and ray trace diagram (bottom) for model M12-14. Presentation and labeling of phases is the same as described in Figure 4.

about 32 km from SH 14 (phase E, Figures 4 and 5). On the SH 14 record section, the 5.5 km/sec travel-time curve continues behind the lower amplitude 6.1 km/sec travel-time curve 32 to 50 km from the shot. The 5.5 km/sec velocity layer extends to about 8.0 km depth below SH 14, decreasing to 6.25 km depth below SH 12. Another 0.5-km-thick high gradient transition zone separates the 5.5 km/sec layer from the 6.1 km/sec layer. As was the case previously, this transition zone was introduced to decrease the amplitudes of rays reflecting off the base of the 5.5 km/sec layer so that the synthetic seismograms more closely match the data.

*Lower crust.* Phase F (Figures 4 and 5), seen 55 to 70 km from both SH 12 and SH 14, is interpreted to be the reflection off the interface between the 6.1 and the 6.75 km/sec layers. The amplitudes for this phase are particularly strong 55 to 60 km from each shot. To focus the energy in this range, phase F was modeled using a 1.2- to 2.0-km-thick transition zone where the velocity increases from 6.15 to 6.68 km/sec. The transition zone dips to the northwest, with its maximum depth ranging from 13.6 (beneath SH 12) to 16.6 km (beneath SH 14). When a first-order discontinuity was used in place of the transition zone, the synthetic seismograms showed the energy from phase F to be distributed evenly along the entire length of the phase, without the concentration of energy 55 to 60 km from the shots.

Additional high-amplitude secondary arrivals recorded in the distance range from 75 to 95 km from both SH 12 and SH 14 (phases G and H, Figures 4 and 5) are interpreted to consist of two distinct phases. The earlier phase G, occurring just behind a very weak first arrival, is interpreted as a reflection off the bottom of the 6.75 km/sec layer, at an average depth of 20 km depth. These data provide no control of velocities for depths greater than this. However, a parallel refraction profile located 10 km to the east of our profile (Holbrook and Mooney, 1986) shows a well-constrained velocity of 7.2 km/sec at this depth; this velocity was assumed for the deep crustal velocity (below 20 km depth) in M12-14. This assumption is reasonable since the two profiles are within the same geologic province. The later phase H is interpreted to be the Moho reflection. The Moho is calculated to be at 27 km, which is the same depth as determined by Hwang and Mooney (1986), who interpreted the SH 14 data assuming flat layers. A Moho velocity of 8.1 km produced a good match to phase H in the synthetic seismograms in Figure 4 and 5.

### SH 13

As mentioned earlier, SH 13 was located 3.85 km east of the nearest station on the line. Since reciprocity could not be used between SH 13 and the other two shots, we used the original model (Model M12-14) as a starting point, and modified it slightly to fit the SH 13 data. The resulting model, referred to as model M13, shows a sedimentary section that is about 0.5 km thinner than that of model M12-14. Model M13 also shows the 5.5 km/sec layer to be about 1 km thicker south of SH 13 and the 6.1 km/sec layer to be thicker by about 2.5 km. Velocity-depth functions in Figure 6 and Table 3 allow for a comparison between the two models.

Model M13 shows slightly faster apparent velocities for phase B (Figure 7), indicating locally higher velocities near SH 13 at the top of the low-velocity zone within the sediments. The cross-over point from phase A to phase B occurs about 0.1 sec later on the SH 13 record than for the other shots, indicating that the first layer is locally thicker beneath SH 13. The depth to basement, the top of the fourth layer, ranges from 4.6 km at the southern end of model M13 to 5.8 km beneath SH 13. In comparison with model M12-14, the top of the basement layer is shallower by 0.4 km beneath SH 14, and 1.0 km shallower beneath SH 12.

Phase E has an apparent velocity of 6.0 km/sec northwest of SH 13; the top of the corresponding refractor (the 6.1 km/sec layer) is about 0.8 km shallower for model M13 than for model M12-14. Southeast of SH 13, phase E has a higher apparent velocity of 6.55 km/sec, indicating a northwest dip for the boundary between the 5.5 and the 6.1 km/sec layer. The modeled depth of this interface at a point 10 km south of SH 13 is 8.65 km, which is 0.25 km deeper than found in model M12-14; however, beneath SH 12, its depth is at 6.3 km, which is 0.3 km shallower than in M12-14. An attempt was made to decrease the dip of this interface

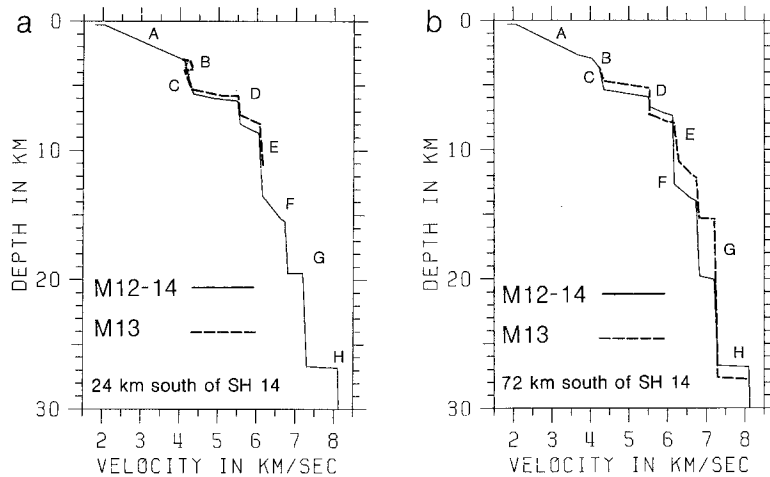


FIG. 6. (a) Velocity-depth functions for models M12-14 and M13, at a point mid-way between SH 14 and SH 13 (Figure 1). Model M13 is constrained only to a depth of 10 km. (b) Velocity-depth functions for models M12-14 and M13 at a point mid-way between SH 13 and SH 12 (Figure 1). Note the velocity discontinuities are shallower for model M13 than for model M12-14. Letters indicate the phases referred to in Figures 4, 5, and 7. Numerical values of the velocity depth functions are given in Table 3.

TABLE 3  
VELOCITY-DEPTH FUNCTIONS USED FOR FIGURE 6

Model M12-14 (24 km SE of SH 14)		Model M13 (24 km SE of SH 14)	
Depth	Velocity	Depth	Velocity
0.00-3.00	1.81-4.09	0.00-3.08	1.81-4.14
3.00-3.51	4.10-4.20	3.08-3.66	4.26-4.36
3.51-5.64	4.15-4.35	3.66-5.28	4.08-4.35
5.64-6.19	4.35-5.20	5.28-5.77	4.35-5.20
6.19-7.97	5.50-5.57	5.77-7.35	5.50-5.57
7.97-8.66	5.57-6.00	7.35-7.80	5.57-6.00
8.66-13.49	6.05-6.15	7.80-10.00	6.05-6.11
13.49-15.49	6.30-6.68		
15.49-19.50	6.73-6.81		
19.50-26.80	7.20-7.30		
26.80-30.00	8.10-8.12		

Model M12-14 (72 km SE of SH 14)		Model M13 (72 km SE of SH 14)	
Depth	Velocity	Depth	Velocity
0.00-2.96	1.86-3.84	0.00-2.96	1.80-3.85
2.96-3.65	4.04-4.23	2.96-3.54	4.03-4.23
3.65-5.41	4.23-4.35	3.54-4.66	4.23-4.35
5.41-5.94	4.35-5.20	4.66-5.18	4.35-5.20
5.94-6.72	5.50-5.53	5.18-7.33	5.50-5.53
6.72-7.39	5.53-6.05	7.33-7.89	5.53-6.05
7.39-12.68	6.13-6.18	7.89-10.78	6.13-6.28
12.68-13.97	6.18-6.68	10.78-12.08	6.28-6.68
13.97-20.03	6.73-6.80	12.08-15.37	6.73-6.81
20.03-26.80	7.20-7.30	15.37-27.80	7.20-7.30
26.80-30.00	8.10-8.12	27.80-30.00	8.10-8.20

by constructing an alternate model using a velocity of 6.4 instead of 6.1 km/sec and using the boundary depth from model M12-14. The velocity of phase E in the alternate model was similar to the observed velocity, but the calculated travel times were 0.3 to 0.4 sec early, indicating the need to place this boundary at a greater

depth. Because the higher apparent velocity for this phase is not seen on the other record sections, we prefer to use a layer velocity of 6.1 km/sec for model M12-14.

The arrivals behind phase E (Figure 7) are interpreted to be the reflections from the top of the 6.75 km/sec layer (phase F). Between SH 13 and SH 12, this interface

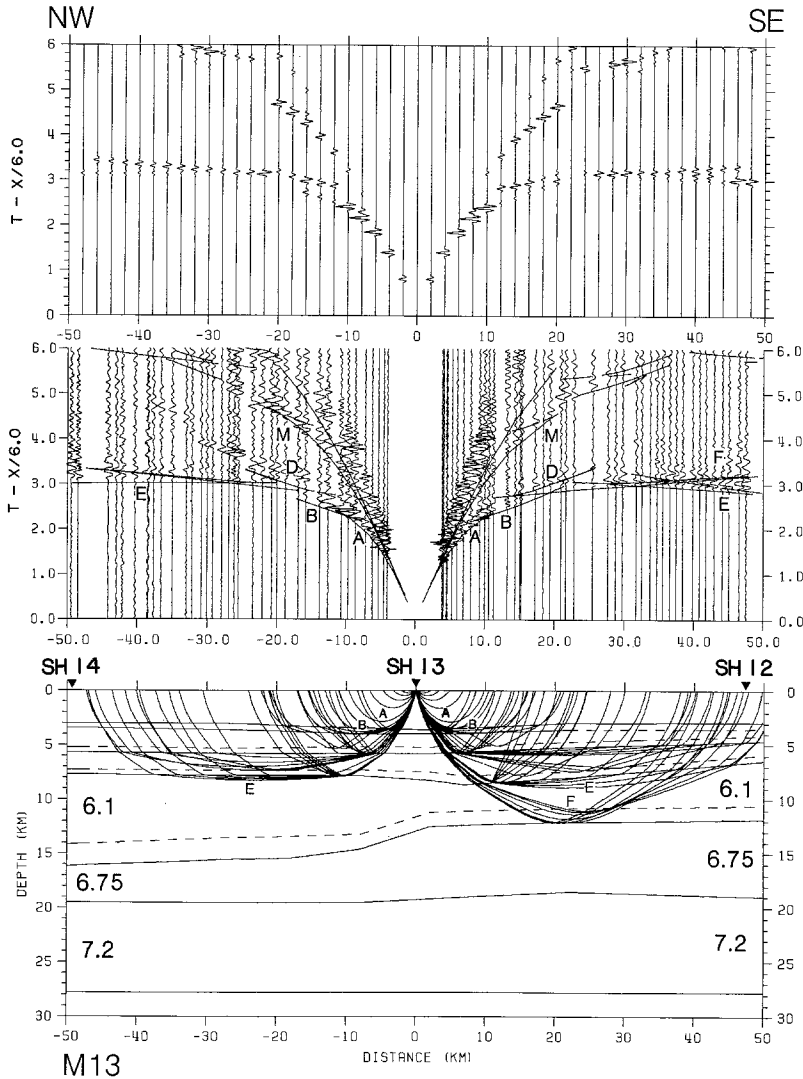


FIG. 7. (SH) 13: Synthetic seismogram (top), true amplitude record section (middle), and ray trace diagram (bottom) for model M13 from SH 13. Presentation is as described in Figure 4.

ranges in depth from 11.8 to 12.5 km, about 1.8 km shallower than for model M12-14. Phase F is not observed from SH 13 to the northwest.

Generally, the amplitudes shown in the synthetic seismograms match well with the amplitudes shown in the data. The most noticeable discrepancy is the lack of strong secondary arrivals in the synthetics that are seen in the data 30 km northeast of SH 13 at a reduced time of about 3.5 sec. (Figure 7). This phase is not seen for SH 13 going southeast or for either of the other shots. It appears to be an anomalous feature that is only seen from the offset SH 13 going north. This feature was not modeled since there is no reversed data to constrain it.

MODEL SOUTHEAST OF SH 12

Both models M12-14 and M13 are extended 50 km southeast of SH 12 to include an interpretation of the unreversed section of the profile. Since station spacing in this area is only 5 km, and since this section is an area of overlapping coverage, rather than reversed coverage, the model for this region is not well constrained. Furthermore, the sparse station spacing makes the identification of phases difficult. This section of the line diverges to the east and cuts diagonally across the strike of

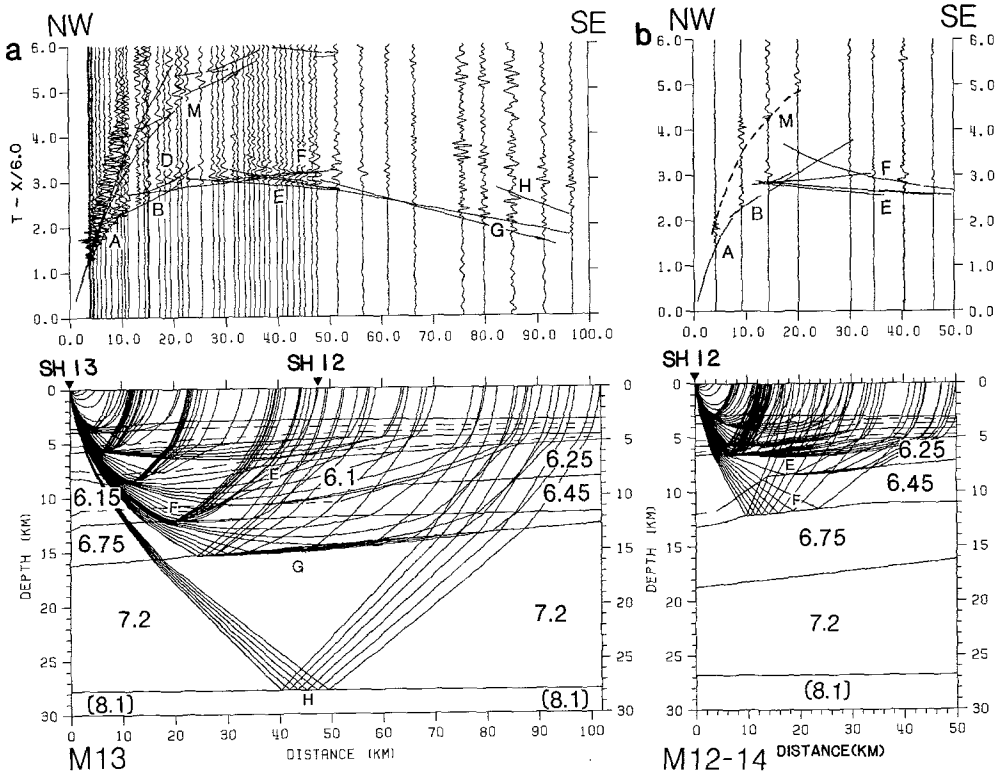


FIG. 8. (a) True amplitude record section (top) and ray trace diagram (bottom) for southern section of model M13 from SH 13. Velocities shown are average velocities within each layer. Phases A, B, D, E, and F correspond to the layers labeled in Figure 6. Phase M is a free-surface multiple refraction. Phase G is the refraction through the 7.2 km layer, and phase H is the reflection off the Moho. (b) True amplitude record section (top) and ray trace diagram (bottom) for southern section of model M12-14 from SH 12. Velocities shown are average velocities (in kilometers/seconds) within each layer. Phases A and B are first arrivals that travel through the near-surface sediments as in the other ray trace diagrams. Phase E denotes refracted arrivals from the 6.25 and 6.45 km/sec layers, and F is the reflection off the top of the 6.75 km/sec layer.

the Valley at about a 20° angle (Figure 1). As a result, rays propagating from SH 13 or SH 14 to the southern end of the model travel through structures east of, rather than under, the main line. This lateral offset is as much as 10 km. Drill hole data in this area indicate that the sediments thin significantly to the east, by as much as 1000 m over a 10 km span, but thin only gradually to the south (Bartow, 1983). When modeling, we kept velocities as consistent as possible with those of the reversed sections of our models and those of the model of Holbrook and Mooney (1986), and adjusted for different apparent velocities by changing the dips of the various interfaces. Figure 8 shows ray trace models and travel-time curves calculated for this section of the model.

The Valley sediments for model M12-14 decrease in thickness from 5.75 km under SH 12 to 4.2 km at the southern end of the model, and from 4.6 to 4.4 km for model M13. Velocities for the most part are extrapolated southeast from beneath SH 12 (Figure 3). One exception is that the velocities at the top of model M12-14 are decreased to 1.4 km/sec at the south end of the model to delay branches E and F 30 to 50 km southeast of SH 12. The 5.5 layer has a fairly constant thickness for M12-14, ranging from 0.75 to 0.90 km, but for model M13 it ranges in thickness from 0.6 to 1.8 km.

Below the 5.5 km/sec layer, both models have two layers with average velocities of 6.25 and 6.45 km/sec, respectively. The 6.25 km/sec layer extends from depths of about 5 to 8 km for model M12-14 and from 5 to 9 km for model M13. The 6.45 km/sec layer extends to about 11 km depth for both models. These two layers replace the 6.2 km/sec layer found north of SH 12. The 6.45 km/sec layer was introduced to advance reflections off the 6.75 km/sec layer from SH 12 (phase F, Figure 8b) and to make this section of the line more consistent with the line of Holbrook and Mooney (1986), which is from 5 to 15 km east of this section of our line.

A relatively high apparent velocity of 7.2 km/sec (phase G, Figure 8a) is seen on the SH 13 record sections 60 to 95 km southeast of the shot. Neither of the other two record sections show such a high apparent velocity at this close a range. To fit this branch on the SH 13 record section, we raised our 7.2 km/sec layer for model M13 from a minimum depth of 16 to 12.5 km. An alternate model that kept the minimum depth of the 7.2 km/sec layer at 16 km used a steep northwest-dipping interface between the 6.4 to 6.75 km/sec layers, with the depth varying from 12.5 beneath SH 12 to 5 km at the south end of the model. This change in depth would be expected to produce a significant gravity anomaly; however, gravity measurements vary by only 25 mgal along the entire length of our profile (Bishop and Chapman, 1967; Robbins *et al.*, 1976). Holbrook and Mooney (1986) show the 7.2 km/sec layer reaching a minimum depth of 16 to 18 km. Model M13 is more consistent with their model and with the gravity data than the alternate model. Model M12-14 uses the same range of depths for the 6.75/7.2 km/sec interface (16 to 19 km) as Holbrook and Mooney (1986). Sparse station spacing and unreversed seismic data make developing a well-constrained model for this region difficult.

#### COMPARISON WITH OTHER PROFILES

Prior to the recording of this profile and the other 10 to 15 km to the east, there were no deep seismic refraction measurements parallel to the axis of the Great Valley. We first discuss these results in the context of the regional profiles, then compare them with the analysis of Hwang and Mooney (1986) and Holbrook and Mooney (1986).

Oppenheimer and Eaton (1984) estimated crustal thickness in central California using travel times of local earthquakes. They estimated a thickness of about 31 km along the strike of our profile, as opposed to our value of 27 km. However, all but one of the seismograph stations used in that study were located in the Coast Ranges and the Sierra Nevada or its foothills. Their estimated thickness for the Great Valley was interpolated from thicknesses calculated for the Coast Ranges and the Sierra Nevada; it did not fully take into account differences in the crustal velocity structure beneath the Great Valley and the Coast Ranges. Oppenheimer and Eaton (1984) presented evidence for a high-velocity ( $\sim 7.4$  km/sec) basal crustal layer beneath the Great Valley. This observation is borne out by the interpretation presented here which includes a 7.2 km/sec lower crustal layer.

The data from SH 14 only was analyzed by Hwang and Mooney (1986), assuming homogeneous, planar layers using synthetic seismograms calculated via the reflectivity method (Kind, 1979; Fuchs and Mueller, 1971). Their velocity model (model HwM) is similar to ours. Figure 8a shows a comparison of model HwM and our preferred model, model M12-14. The major differences are: (1) the low-velocity zone at the base of the sediments is 1.4 km thick in model HwM, but 2.2 km thick in model M12-14; (2) model HwM does not use any high-velocity, gradient transition zones, only first-order discontinuities; (3) model M12-14 uses a 2.5-km-thick basement layer with a velocity of 5.5 km/sec overlying a 6-km-thick layer of velocity 6.1 km/sec, whereas model HwM uses a single layer ranging in depth from 6.2 to 16.2 km, with velocities ranging from 5.7 to 6.3 km/sec; (4) both models have a first-order discontinuity in the lower crust—however, model M12-14 shows the velocity

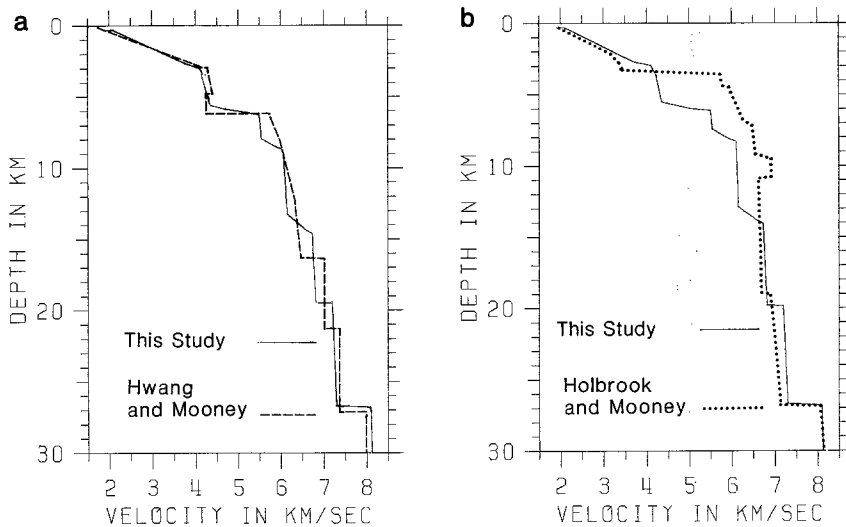


FIG. 9. (a) Comparison of typical velocity-depth functions between the preferred model of this study (model M12-14) and that of Hwang and Mooney (1986). (b) Comparison of typical velocity-depth functions between model M12-14 and the model of Holbrook and Mooney (1986).

contrast to be from 6.8 to 7.2 km/sec at a depth of 19.5 km, while model HwM shows it to be from 7.0 and 7.4 km/sec at 21.3 km depth. Both models place the Moho at about 27 km depth. Generally, the one-dimensional model HwM shows slightly higher velocities and greater depths to interfaces than our model; this discrepancy may be due to the neglect of dip effects in their one-dimensional modeling method.

Figure 9b shows a comparison between our preferred model (model M12-14) and that of Holbrook and Mooney (1986) for a profile parallel and 10 to 15 km east of ours (Figure 1). In general, their model (model HoM) shows a thinner sedimentary section and higher upper crustal velocities than model M12-14, although the lower crust is very similar in both models. Model HoM shows the Great Valley sediments to be 3.2 km thick, as opposed to about 6 km thick for model M12-14. This is expected, since the sediments are known to thin to the east (Bartow, 1983). Model HoM also shows the sediments to be underlain by a 5.5 km/sec layer about 1 km thick; model M12-14 shows this 5.5 km/sec layer to be 2.5 km thick. Beneath this layer, model HoM shows velocities ranging from 6.0 to 6.3 km/sec extending to 7 km in depth. From 7 to 11 km depth, model HoM shows velocities ranging from 6.5

to 7.0 km/sec. Model M12-14 does not show velocities in this range above a depth of 14.5 km. From 11 to 19 km depth, model HoM show a near-constant velocity of 6.75 km/sec. Model M12-14 uses a velocity of 6.1 km/sec from 8.5 to 14.5 km deep, and a velocity of 6.75 km/sec extending to 19.5 km deep. Both models use velocities ranging from 7.1 to 7.3 km/sec above the Moho. The Moho depth is constant at 27 km in model 12-14, whereas model HoM has the Moho dipping to the southeast, with depths ranging from 26 to 28.5 km.

## DISCUSSION

Our final two-dimensional velocity model (Figure 3a) shows velocities ranging from 1.7 to 7.2 km/sec, which corresponds to a wide range of geologic materials. Some inferences of the geologic composition of each layer may be made on the basis of previous geophysical work and the geologic setting.

Cenozoic sedimentary deposits, and Mesozoic marine sediments of the Great Valley sequence comprise the top 6 km of the crust and show velocities ranging from 1.7 to 4.5 km/sec. The structure and lithology of the sedimentary rocks of the Great Valley are already well constrained from drill-hole data (Bartow, 1983) and extensive seismic reflection profiling conducted for the purpose of resource exploration. We have determined the average velocity structure and thickness of this section beneath our profile. The most notable feature of this velocity structure is the high-velocity gradient (0.7 km/sec/km) in the upper 3 km and the much lower velocity gradient below that depth. We have observed some evidence for a modest velocity inversion (low-velocity zone) at the base of the sediments. This velocity inversion is consistent with that obtained within the Great Valley sequence 120 km to the southeast by Walter (1985).

The Great Valley sequence rests on a 1.0 to 2.5-km-thick layer with a velocity of 5.5 km/sec. We do not include this layer as part of the Great Valley sequence because it is at least 0.5 km/sec higher in velocity than has been reported elsewhere for the Great Valley sequence (Meltzer *et al.*, 1985; Walter, 1985). A velocity of 5.5 km/sec is appropriate for rocks of the Franciscan assemblage (Walter and Mooney, 1982; Blümling and Prodehl, 1983), fractured crystalline rocks, or serpentinized ophiolite. It is, however, a lower velocity than measured in most unaltered crystalline rocks (Birch, 1960; Christensen, 1982). Wentworth *et al.* (1984) interpreted seismic refraction and reflection data across the Great Valley-Coast Range boundary as showing a tectonic wedge of Franciscan rocks, which they suggest is thrust beneath the Great Valley sequence. Their interpretation shows this wedge as pinching out approximately beneath our line; in contrast, our result may be interpreted as showing 2 km of Franciscan rocks at this location. Alternatively, the fact that the 5.5 km/sec layer is also seen below the parallel seismic refraction profile 10 to 15 km to the east suggests that it consists of fractured crystalline basement rocks rather than a Franciscan wedge.

The 5.5 km/sec layer rests upon a 6-km-thick layer having an average velocity of 6.1 km/sec. The composition of this layer is problematic, as it is higher in velocity than typical Franciscan assemblage, but significantly lower in velocity than oceanic crustal rocks hypothesized to underlie the Great Valley (Cady, 1975). This velocity is also substantially lower than the 6.6 to 6.8 km/sec material upon which the Franciscan assemblage of the Diablo Range rests (Walter and Mooney, 1982; Blümling and Prodehl, 1983). The 6.1 km/sec layer could consist of a wide range of rock types, including plutonic, metamorphic, and welded volcanoclastic rocks. Since this layer has no velocity equivalent in the Coast Ranges to the west, it is more

appropriate to correlate this layer with the rocks exposed to the east where a profile recorded in the northern Sierra foothills (Speith *et al.*, 1981) shows upper crustal velocities of 6.2 km/sec. Therefore, we hypothesize that this layer is composed of metamorphic and/or granitic rocks such as are exposed in the foothills of the Sierra Nevada (Jennings, 1977).

The lower crust consists of two layers with average velocities of 6.7 and 7.2 km/sec, and average thicknesses of 6 and 7 km, respectively. The layer with a velocity of 6.75 km/sec may be correlated with a layer of similar velocity found at a depth of 12 to 16 km beneath the Franciscan assemblage of the central Coast Ranges (Walter and Mooney, 1982; Blümling and Prodehl, 1983). Lin and Wang (1981) and Walter and Mooney (1982) discuss in detail the possible composition of rocks with a velocity of 6.7 km/sec beneath the Coast Ranges. These authors showed that a wide range of rocks fit these velocities, but in view of the marine metasedimentary rocks (Franciscan assemblage) which overlie the 6.7 km/sec layer in the Coast Ranges and the occurrence within the Franciscan assemblage of blocks of gabbroic rocks, mafic rocks derived from oceanic crust is the most plausible composition. A similar composition of the 6.75 km/sec layer is possible for the Great Valley, but the problem remains to explain the association of the 6.75 km/sec layer with the 7.2 km/sec layer beneath it, and with the overlying 6.1 km/sec layers. A second possibility is that the 6.75 km/sec layer, along with the overlying 6.1 km/sec layer, is correlated with the metamorphic and igneous rocks of the Sierra-Nevada foothills, since Speith *et al.* (1981) reported crustal velocities of 6.2 and 6.6 km/sec in the northern Sierra-Nevada foothills, approximately 200 km north of our study area.

The 7.2 km/sec layer may have an origin similar to the 6.75 km/sec layer, but is evidently denser and more mafic in composition. This material may represent oceanic crust, or possibly mafic igneous rocks that have been magmatically underplated to the originally thinner crust of the Great Valley.

Amplitude modeling of this data has led us to propose a crustal structure with several high-velocity gradient transition zones (phases E and F, Figure 6). These transition zones may be indicative of either a gradual change in metamorphic grade with depth, or a layered intrusive zone separating the two layers. The first-order discontinuities indicate a relatively rapid change in rock type with depth, but it is unlikely that the discontinuities G and H are as simple as our model shows. Discontinuity H is the crust/mantle boundary, and numerous studies have demonstrated that it is a laminated zone rather than the simple step we show (e.g., Meissner, 1973; Hale and Thompson, 1982).

The total crustal thickness along this profile is 27 km. If the 6 km sedimentary column and the 5.5 km/sec layer are subtracted from this, a 19-km-thick crystalline crust remains, with average velocities of 6.1, 6.7, and 7.2 km/sec (Figure 3). This crustal velocity structure is not similar to either typical oceanic or continental crust, and we seek an atypical setting for its formation. Two previous suggestions are that the Great Valley formed to the west of the Sierra Nevada arc as a forearc basin (Dickinson and Seely, 1979) or as a backarc basin (Schweickert and Cowan, 1975). While we cannot distinguish these two hypotheses on the basis of the crustal velocity structure, our results do require an origin of the crust beneath our profile in a setting that provides a 19-km-thick crystalline crust, including a 13-km-thick, dense lower crust (6.7 and 7.2 km/sec). Formation as greatly thickened oceanic crust in a marginal basin appears to be the best model.

Further constraints on the origin and three-dimensional velocity structure of the crust of the Great Valley will be obtained from the analysis of the perpendicular-

to-strike seismic refraction and reflection profiles, and we defer a comprehensive discussion of the origin of the crustal structure obtained here until the analysis of those profiles has been completed and synthesized with the potential field and geologic data.

#### ACKNOWLEDGMENTS

Many people have contributed to this study in various ways. We thank A. Boken, J. M. Bonomolo, E. E. Criley, K. E. Harrington, L. R. Hoffman, R. P. Meyer Jr., G. A. Molina, J. M. Murphy, J. R. VanShaaek, and V. D. Sutton for their efforts in the field. E. L. Ambos, A. W. Walter, C. M. Wentworth, L. J. Hwang, W. S. Holbrook, and D. Whitman have contributed many ideas during the analysis of the data. Our ray trace modeling was accomplished using software prepared by J. H. Luetgert. Careful reviews by R. L. Nowack, A. W. Walter, and C. M. Wentworth substantially improved this paper.

#### REFERENCES

- Bartow, J. A. (1983). Map showing configuration of the basement surface, northern San Joaquin Valley, California, U.S. Geological Survey Miscellaneous Field Studies Map MF-1430, 1:250,000.
- Birch, F. (1960). The velocity of compressional waves in rocks to 10 kilobars, *J. Geophys. Res.* **65**, 1083–1102.
- Bishop, C. C. and R. H. Chapman (1967). Bouguer Gravity Map of California, Santa Cruz Sheet, California Division of Mines and Geology, Sacramento, California, 1:250,000.
- Blümling, P. and C. Prodehl (1983). Crustal structure beneath the eastern part of the Coast Ranges (Diablo Range) of central California from explosion-seismic and near-earthquake data, *Phys. Earth Planet. Interiors* **31**, 313–326.
- Cady, J. W. (1975). Magnetic and gravity anomalies in the Great Valley and western Sierra Nevada metamorphic belt, California, *Geol. Soc. Am. Spec. Paper* **168**, 56 pp.
- Christensen, N. I. (1982). Seismic velocities, in *Handbook of Physical Properties of Rocks*, vol. 2., R. S. Carmichael, Editor, CRC Press, Boca Raton, Florida, 1–228.
- Dickinson, W. R. (1976). Sedimentary basins developed during evolution of Mesozoic-Cenozoic archtrench system in western North America, *Can. J. Earth Sci.* **13**, 1268–1287.
- Dickinson, W. R. and D. R. Seely (1979). Structure and stratigraphy of forearc regions, *Am. Assoc. Petrol. Geol. Bull.* **63**, 2–31.
- Eaton, J. P. (1963). Crustal structure from San Francisco, California, to Eureka, Nevada, from seismic-refraction measurements, *J. Geophys. Res.* **68**, 5789–5806.
- Eaton, J. P. (1966). Crustal structure in northern and central California from seismic evidence, in *Geology of Northern California*, E. H. Bailey, Editor, *Calif. Div. Mines Geol. Bull.* **190**, 419–426.
- Fuchs, K. and G. Mueller (1971). Computation of synthetic seismograms with the reflectivity method and comparison with observations, *Geophys. J. R. Astr. Soc.* **23**, 417–433.
- Fuis, G. S., W. D. Mooney, J. H. Healy, G. A. McMechan, and W. J. Lutter (1984). A seismic refraction survey of the Imperial Valley region, California, *J. Geophys. Res.* **89**, 1165–1189.
- Hale, L. D. and G. A. Thompson (1982). The seismic reflection character of the continental Mohorovičić discontinuity, *J. Geophys. Res.* **87**, 4625–4635.
- Healy, J. H. (1963). Crustal structure along the coast of California from seismic refraction measurements, *J. Geophys. Res.* **68**, 5777–5787.
- Holbrook, W. S. and W. D. Mooney (1986). The crustal structure of the Great Valley, California, from seismic refraction measurements (submitted for publication).
- Hwang, L. and W. D. Mooney (1986). Velocity and *Q* structure of the Central Valley, California, based on synthetic seismogram modeling of seismic refraction data, *Bull. Seism. Soc. Am.* **76**, 1053–1067.
- Jennings, C. W. (1977). Geologic Map of California, California Division of Mines and Geology, Sacramento, California, scale 1:750,000.
- Kind, R. (1979). The reflectivity method for a buried source, *J. Geophys.* **45**, 373–380.
- Lin, W. and C. Y. Wang (1980). *P*-wave velocities in rocks at high pressure and temperature and the constitution of the central California crust, *Geophys. J. R. Astr. Soc.* **61**, 379–400.
- McMechan, G. A. and W. D. Mooney (1980). Asymptotic ray theory and synthetic seismograms for laterally varying structure: theory and application to the Imperial Valley, California, *Bull. Seism. Soc. Am.* **70**, 2021–2035.
- Meissner, R. (1973). The “Moho” as a transition zone, *Geophys. Surv.* **1**, 195–216.
- Meltzer, A. S., A. R. Levander, and W. D. Mooney (1985). Interpretations of seismic refraction profiles east of Livermore, California (abstract), *EOS* **66**, 973.

- Oppenheimer, D. H. and J. P. Eaton (1984). Moho orientation beneath Central California from regional earthquake travel times, *J. Geophys. Res.* **89**, 10,267–10,282.
- Prodehl, C. (1979). Crustal structure of the western United States, *U.S. Geol. Surv. Profess. Paper 1034*, 74 pp., 3 plates.
- Robbins, S. L., H. W. Oliver, and K. D. Holden (1976). Bouguer Gravity Map of California, San Jose Sheet, California Division of Mines and Geology, Sacramento, California, scale 1:250,000.
- Schweickert, R. A. and D. S. Cowan (1975). Early Mesozoic tectonic evolution of the western Sierra Nevada, California, *Geol. Soc. Am. Bull.* **86**, 1329–1336.
- Speith, M. A., D. P. Hill, and R. J. Geller (1981). Crustal structure in the northwestern foothills of the Sierra Nevada from seismic refraction experiments, *Bull. Seism. Soc. Am.* **71**, 1075–1087.
- Stewart, S. W. (1968). Preliminary comparison of seismic travel times and inferred crustal structure adjacent to the San Andreas fault in the Diablo and Gabilan Ranges of central California, In *Proceedings of Conference on Geologic Problems of San Andreas Fault Systems*, W. R. Dickinson and A. Grantz, Editors, *Stanford University Publication of Geological Science* **11**, 218–230.
- Walter, A. W. (1985). Velocity structure near Coalinga, California, in *Mechanics of the May 2, 1983, Coalinga, California, Earthquakes*, M. J. Rymer and W. L. Ellsworth, Editors, *U.S. Geol. Surv., Open-File Rept. 85-44*, 10–18.
- Walter, A. W. and W. D. Mooney (1982). Crustal structure of the Diablo and Gabilan Ranges, central California: a reinterpretation of existing data, *Bull. Seism. Soc. Am.* **72**, 1567–1590.
- Wentworth, C. M., M. C. Blake, Jr., D. L. Jones, A. W. Walter, and M. D. Zoback (1984). Tectonic wedging associated with emplacement of the Franciscan assemblage, California Coast Ranges, in *Franciscan Geology of Northern California: Society of Economic Paleontologists and Mineralogists*, vol. 43, M. C. Blake Jr., Editor, Pacific Section, 163–173.
- Wentworth, C. M., M. D. Zoback, and J. A. Bartow (1985). Tectonic setting of the Coalinga earthquakes from seismic reflection profiles: a progress report, in *Mechanics of the May 2, 1983, Coalinga, California, Earthquake*, M. J. Rymer and W. L. Ellsworth, Editors, *U.S. Geol. Surv., Open-File Rept. 85-44*, 19–30.
- Whitman, D., A. W. Walter, and W. D. Mooney (1985). Crustal structure of the Great Valley, California: cross profile (abstract), *EOS* **66**, 973.
- Zoback, M. D. and C. M. Wentworth (1985). Crustal studies in central California using an 800-channel seismic reflection recording system, in *Reflection Seismology: A Global Perspective*, M. Barazangi and L. Brown, Editors, *American Geophysical Union Geodynamic Series* **13**, 183–196.

U.S. GEOLOGICAL SURVEY  
345 MIDDLEFIELD ROAD  
MS 977  
MENLO PARK, CALIFORNIA 94025

Manuscript received 6 March 1986